Asian Journal of Chemistry; Vol. 38, No. 8 (2026), 2131-2145
ASIAN JOURNAL OF CHEMISTRY
https://doi.org/10.14233/ajchem.2026.36406

Synthesis of Triazolylazetidinones as Promising Antitubercular Agents: Computational and Experimental Validation Targeting Polyphosphate Kinase 2

TRIVENI SINGIRISETTY[1,2], VIJAYA BHASKAR KURUBA[3], AZGER DUSTHACKEER VIJAYAN NYNAR[4], NARESH BABU CHILAMAKURU[5] and VIJAYA JYOTHI MALLELA[5,*]

[1]Manipal Academy of Higher Education, Manipal-576104, India
[2]RERDS-CPR, Raghavendra Institute of Pharmaceutical Education and Research Campus, Ananthapuramu-515721, India
[3]Department of Pharmaceutical Chemistry, Manipal College of Pharmaceutical Sciences, Manipal Academy of Higher Education, Manipal-576104, India
[4]ICMR-National Institute for Research in Tuberculosis (NIRT), Chennai-600031, India
[5]Department of Pharmaceutical Chemistry, RERDS-CPR, Raghavendra Institute of Pharmaceutical Education and Research campus, Ananthapuramu-515721, India

*Corresponding author: E-mail: drmvjyothiriper@gmail.com

Received: 9 May 2026 *Accepted*: 11 July 2026 *Published online*: 7 August 2026 AJC-22440

A series of novel 1,2,4-triazole-azetidin-2-one hybrids (**A_1-A_{12}**) were designed and synthesised as potential anti-tubercular agents. The compounds were synthesised *via* Schiff base formation followed by cyclocondensation reactions. The compounds were studied as anti-tubercular agents against polyphosphate kinase 2 (PPK2), an enzyme involved in nucleotide regulation in *Mycobacterium tuberculosis*. A three-dimensional model of PPK2 was generated and examined by molecular dynamics studies. Docking studies indicated favourable interactions of some compounds with amino acid residues ASN131, GLU136, LYS75 and ARG127 in the active site of PPK2, supporting their possible role as PPK2 inhibitors. ADMET simulation analysis revealed favourable physico-chemical and pharmacokinetic parameters, satisfying the criteria for oral drug-likeness. The anti-tubercular activity of compounds **A_1-A_{12}** was evaluated against *M. tuberculosis* H37Rv using the minimum inhibitory concentration (MIC) method. Compounds **A_{11}** and **A_{12}** exhibited the highest activity with MIC values below 7.81 µg/mL, while the remaining derivatives showed moderate to weak activity. Cytotoxicity studies on Vero cells demonstrated concentration-dependent effects, and IC_{50} values indicated acceptable selectivity for compounds **A_1** and **A_{12}**. Acute oral toxicity studies in mice established an LD_{50} value of 300 mg/kg. Histopathological examination of major organs revealed no significant structural changes at tolerated doses.

Keywords: Triazole, Azetidinones, Polyphosphate kinase 2, Molecular docking, ADMET profiling, Antitubercular activity.

INTRODUCTION

Azetidinones are nitrogen-containing saturated four-membered lactams, have versatility against a wide range of microorganisms and their efficacy for acting upon the central nervous system make them valuable templates for medicinal chemistry [1]. Historically, β-lactam antibiotics (penicillins and cephalosporins) have led to a significant improvement within the treatment of infections caused by bacteria [2,3]. Nevertheless, with the advent of resistant bacterial strains, there has been a pressing demand for new β-lactam agents, especially monocyclic azetidinones [4]. Moreover, the four-membered-ring system of β-lactams is amenable for various modifications and can be used for preparing a range of biologically active compounds [5]. These compounds can be synthesised by cyclocondensation reactions of Schiff bases [6].

Recent studies have identified 1,2,4-triazoles and their hybrids as promising antimycobacterial scaffolds and reporting low micromolar activity against *M. tuberculosis* (Mtb) [7,8]. Azetidin-2-ones (β-lactams) are also an important class of heterocycles [9] with extensive literature in antibacterial chemotherapy and expanding roles as antimicrobial [10,11], antifungal [12,13], anticonvulsants [14,15], anti-inflammatory [16,17], antitubercular and enzyme inhibitors [18,19]. Modern studies on triazole-incorporated and azetidinone-based like

azetidin-2-one analogues have explored that appropriate steric and electronic modifications at the β-lactam ring significantly modulate antimycobacterial potency [20,21] and often yielding compounds with excellent minimum inhibitory concentrations (MICs) and satisfactory safety profiles. These remarks support the design of hybrid molecules combining 1,2,4-triazole and azetidin-2-one [22] frameworks to connect potential synergistic effects.

Concurrently, the development of 1,2,4-triazoles has been predictable as another fortunate nitrogen-containing heterocycle that has been widely explored for its diversified pharmacological applications [23]. These include antibacterial, antifungal, antitumor, anti-inflammatory and neuroprotective effects [24,25]. The functional characteristics, especially the high electron density and H-bonding nature, make notable contributions towards their interaction with biological targets. The triazoles can often serve as basic skeletons or bioisosteres in designing drugs and can be found in many marketed drugs. Although they have been widely explored, up-to-date detailed reviews on the synthesis and medicinal applications of derivatives of 1,2,4-triazoles remain scarce in the past few years [26]. As both azetidinones and 1,2,4-triazoles display high medicinal value, the present investigation deals with the synthesis, characterisation, molecular docking studies, ADMET simulation, biological screening and acute toxicity studies of the newly designed hybrid compounds incorporating these moieties. The strategy is aimed at exploring the combined benefits of these two heterocyclic moieties towards designing improved scaffolds with enhanced medicinal properties. *Mtb* H37Rv is an extremely potent human pathogen that possesses highly developed strategies for its replication and survival within the lungs while avoiding the immune system [27,28].

In addition to the discovery of novel scaffolds, non-classical targets related to the persistence and stress response of bacteria, especially those of *Mtb*, have preserve increasing attention [29]. Polyphosphate kinases (PPKs), which modulate inorganic polyphosphate (polyP), are strongly associated with energy metabolism, stress resistance, biofilm formation and virulence of *Mtb* [30]. More specifically, polyphosphate kinase 2 (PPK2), which is strongly associated with the virulence of *Mtb*, has been shown to be a promising target for the development of antitubercular agents, as its deletion or knockdown has been found to inhibit the survival and pathogenicity of *Mtb*. To the best of our knowledge, no previous systematic study has reported the design and biological evaluation of triazolyl-azetidinone derivatives specifically targeting *M. tuberculosis* PPK2 [31,32].

Although several triazole-, azetidinone- and triazole-azetidinone based derivatives have demonstrated antibacterial activity, these investigations have predominantly focused on conventional mycobacterial targets such as InhA, DprE1, DNA gyrase and cell wall biosynthetic enzymes. Comparatively, the potential of these scaffolds against PPK2 has remained largely unexplored. PPK2 is an attractive non-classical therapeutic target since it regulates polyphosphate metabolism, bacterial persistence, stress adaptation and virulence without having a close human homologue. Therefore, targeting PPK2 may provide an opportunity to develop antitubercular agents with a novel mechanism of action while reducing the likelihood of cross-resistance with currently available drugs. In this context, the present study represents the first systematic effort to design, synthesise and biologically evaluate triazolyl-azetidinone derivatives as potential PPK2-directed antitubercular agents [33].

EXPERIMENTAL

All chemicals and reagents used in this study were of analytical grade and procured from reputed suppliers such as Loba Chemie, Himedia and Thermo-Fisher. Melting points were determined in an open capillary tube using a digital melting point apparatus and are uncorrected. Homology modelling was performed using Schrödinger Prime and docking studies were performed using Glide (v2024_1). ADMET properties were predicted using the ADMETlab 2.0 web tool by uploading the SMILES strings of all synthesised compounds. IR spectra were recorded on a Bruker Alpha Fourier-transform infrared by the KBr pellet technique. ^{1}H NMR and ^{13}C NMR spectra were recorded on a Bruker NMR spectrometer using DMSO and $CDCl_3$ as a solvent and TMS as an internal standard. Mass spectra were recorded on an APEX mass spectrum using the electron scattering ionisation method.

Target selection, homology modelling and validation: The crystal structure of polyphosphate kinase2 of *Mtb* is not available in Protein Data Bank (PDB). The amino acid sequence FASTA is available in National Centre for Biotechnology Information with reference sequence: WP_003416928.1 with 295 amino acid residues (FASTA) [34,35]. Based on the BLAST analysis performed using the NCBI database, a suitable template was identified for protein modelling. The three-dimensional structure of the target protein was generated using the Structure Prediction Wizard module of Schrödinger Prime. The predicted model was subsequently validated using the PROCHECK web server and its structural stability was further assessed through molecular dynamics simulation studies [36,37].

Molecular docking studies

Ligand preparation: The structures drawn in ChemDraw software were imported into Maestro 13.9 in .MOL format. All ligands were selected into the workspace and they were subjected to Ligprep and converted from 2D to 3D with minimisation energy (OPLS4 force field) with the default settings [38].

Protein preparation and receptor grid generation: By following the standard procedure, 5LLB_C protein and PPK2 modeled proteins were pre-processed, optimised and minimised with the help of the OPLS4 force field by using the protein preparation wizard. The Ramachandran plot of the 5LLB_C and PPK2 modeled proteins showed favoured, allowed and disallowed regions of the amino acids represented in Fig. 1. The active/binding site in the minimised protein of the 5LLB_C and PPK2 modeled protein was identified by site map analysis. In sitemap analysis, 2 active sites with site scores of 1.015 and 0.596, were observed in 5LLB. Site 1 is selected due to its higher site score with a size of 218, a Dscore of 0.930, a volume of 686.343, a phobic score of 0.344, a philic score of 1.356 and a don/acc 0.485. A grid was gener-

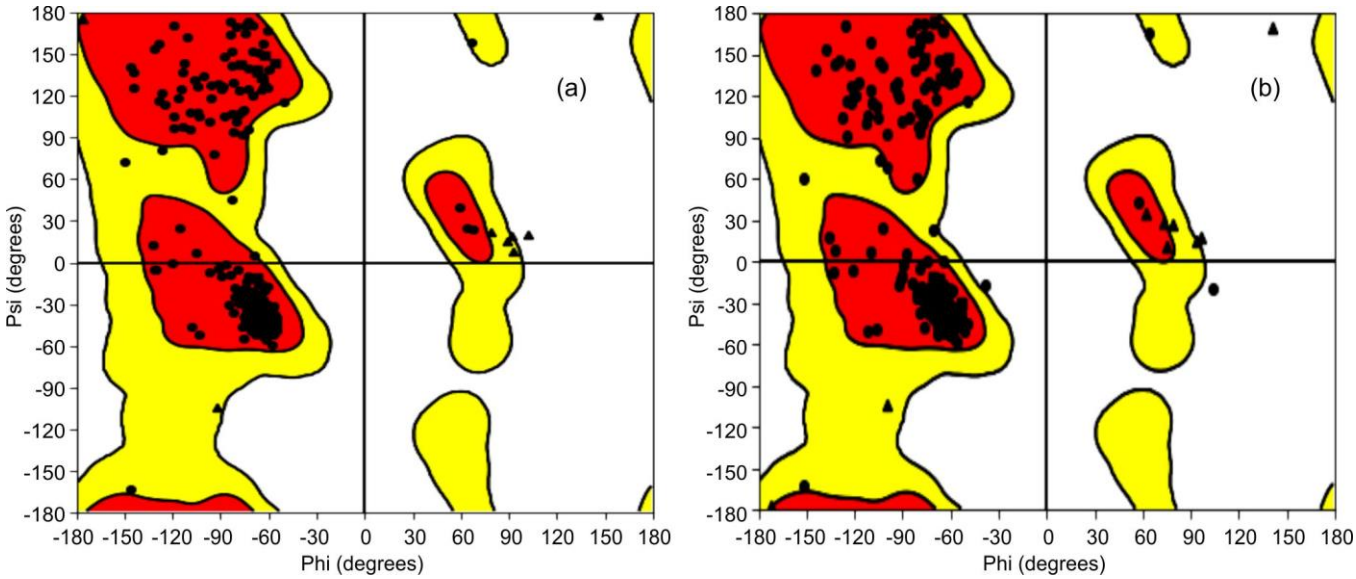

Fig. 1. Ramachandran plot of the protein 5LLB_C and PPK2 modeled protein shows ψ and ϕ angles of amino acid residues

ated with X, Y and Z coordinates -2.27, -10.09 and -4.47, with box lengths in X, Y and Z of 20, 30 and 20 Å, respectively. In sitemap analysis of PPK2 modelled protein, 5 sites with site scores of 1.007, 0.835, 0.834, 0.573 and 0.569 were observed. Among these 5 sites, sitemap 1 has a large size of 215, a Dscore of 0.930, a volume of 581.185, a phobic score of 0.300, a philic score of 1.335 and a don/acc. Generated a grid surrounding sitemap 1 protein entry, with X, Y and Z coordinates -2.16, -9.84 and -5.15, with box lengths in X, Y and Z of 15, 15 and 15 Å, respectively.

Ligand docking: Ligand docking was performed using the virtual screening workflow in the Schrödinger suite. The Glide grid and LigPrep output files were imported from the working directory and docking calculations were carried out using the Standard Precision (SP) mode. The docked poses were ranked according to their docking scores and binding energies, and the interactions of the ligands with the amino acid residues present in the active sites of both target proteins were analysed [39].

ADMET properties calculation: ADMETlab 2.0 is an advanced iteration of the widely utilised ADMETlab, designed for comprehensive assessment of ADMET properties, along with various physico-chemical properties and medicinal chemistry attributes [40,41].

General procedure for the synthesis of Schiff bases (T_1-T_{12}): 4-Amino-1,2,4-triazole (1.68 g, 0.02 mol) (**1**) taken in a tube of parallel synthesiser, was dissolved in 15 mL methanol. To each tube was added 0.02 mol of aromatic aldehyde and a catalytic amount (2-4 drops). The mixture was refluxed for 4 h. and then cooled on ice. The separated solid product was isolated by filtration and recrystallised from ethanol [42,43]. Melting points and yields are shown in Table-1.

General procedure for the synthesis of triazolo-azetidine-2-ones (A_1-A_{12}): To a solution of the corresponding Schiff base (T_1-T_{12}, 0.01 mol) in 10 mL of dioxane, triethylamine (0.349 mL, 0.025 mol) was added. Chloroacetyl chloride (0.4 mL, 0.025 mol) was then added dropwise while maintaining the temperature between 0-5 ºC. The reaction mixture was stirred for 6 h and subsequently allowed to stand at room temperature for 2 days. The reaction mixture was poured into crushed ice to give the solid, which was filtered, dried and recrystallised from ethanol (**Scheme-I**).

TABLE-1
PHYSICO-CHEMICAL DATA OF
SYNTHESIZED SCHIFF BASES (T_1-T_{12})

Compd.	m.f.	m.w.	m.p. (ºC)	Yield (%)
T_1	$C_9H_7NO_2$	217.06	270-271	54.30
T_2	$C_{10}H_{10}N_4O_2$	218.08	250-251	32.11
T_3	$C_9H_8N_4O$	188.07	207-208	59.00
T_4	$C_9H_7N_5O_2$	217.06	250-252	41.90
T_5	$C_9H_6Cl_2N_4$	240.00	170-172	25.70
T_6	$C_{11}H_6N_4O_3$	248.09	295-297	20.66
T_7	$C_{11}H_9N_5$	211.09	200-202	40.70
T_8	$C_{11}H_{13}N_5$	215.12	100-101	40.00
T_9	$C_{11}H_6N_4O_2$	232.10	110-112	11.06
T_{10}	$C_{11}H_7N_4O$	202.09	97-99	62.30
T_{11}	$C_{11}H_7N_4O_2$	232.10	195-197	37.00
T_{12}	$C_9H_8N_4O$	188.07	255-256	66.40

3-Chloro-4-(4-nitrophenyl)-1-(4*H*-1,2,4-triazol-4-yl)-azetidine-2-one (A_1): Yield: 54%; m.p. 195-197 ºC; Elemental anal. of $C_{11}H_8ClN_5O_3$: calcd. (found) %: C, 44.99 (45.01); H, 2.75 (2.74); Cl, 12.07 (12.06); N, 23.85 (23.87); O, 16.34 (16.32).IR (KBr, ν_{max}, cm^{-1}): 1710.71 (C=O), 1510.41, 1391.47 (C-N, 3º NH_2), 1343.45 (NO_2), 847.30 (C-N, NO_2), 751.19 (C-Cl); ^{1}H NMR (500 MHz, DMSO-d_6, δ ppm): 3.3860 (s, 1H, azetidin-2-one), 8.0966-8.1188 (d, 2H, J = 1.9 Hz, Ar-H), 8.3903-8.4124 (d, 2H, J = 2.2 Hz, Ar-H), 9.2135 (s, 1H, triazole), 9.2694 (s, 1H, triazole); ^{13}C NMR (100 MHz, DMSO-d_6, δ ppm): 51.05 (C-Cl), 64.37 (CH, azetidinone), 126.90-132.51 (Ar-C), 142.35, 149.96 (Ar-C), 151.94, 152.65 (triazole), 173.77 (C=O); MS (ESI): *m/z*: 294.10 $[M]^+$.

3-Chloro-4-(2-hydroxyphenyl)-1-(4*H*-1,2,4-triazol-4-yl)azetidine-2-one (A_3): Yield: 16.1%; m.p. 180-181 ºC; Elemental anal. of $C_{11}H_9ClN_4O_2$: calcd. (found) %: C, 49.92 (49.90); H, 3.43 (3.45); Cl, 13.40 (13.40); N, 21.17 (21.14);

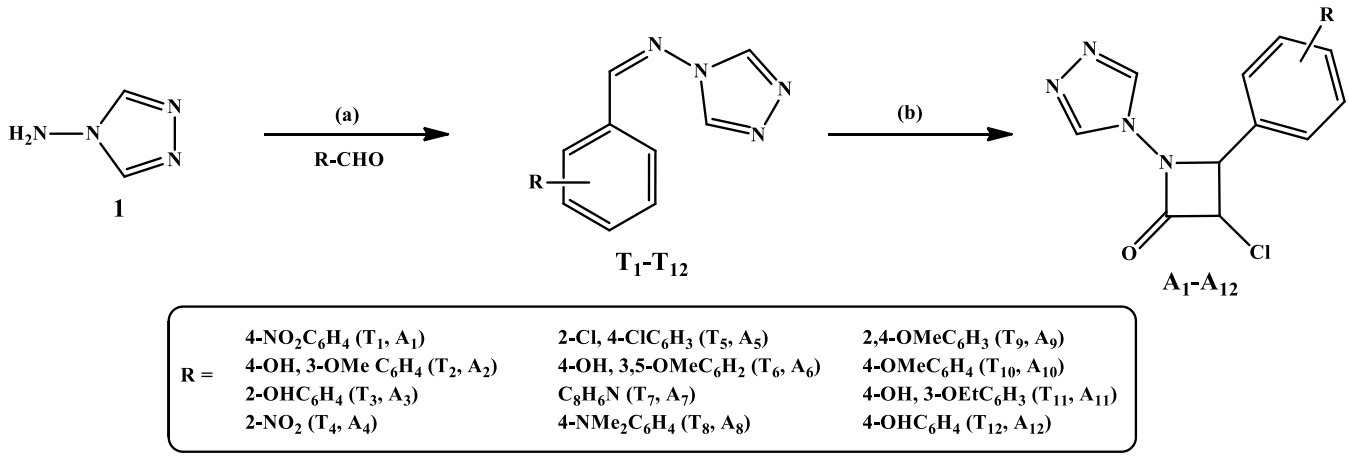

Scheme-I: Synthesis of triazolylazetidinone derivatives **A1-A12** [Reaction conditions: (a) Glacial acetic acid, MeOH, 80 ºC, 4-6 h; (b) chloroacetyl chloride, dioxane, triethylamine, 0-5 ºC, 6 h stirring]

O, 12.08 (12.11); IR (KBr, ν_{max}, cm^{-1}): 3539.98 (O-H), 1682.49 (C=O), 1449.82 (O-H *def.*); 1366.01 (C-N, 3º NH_2), 1248.45 (C-O), 754.71 (C-Cl); ^{1}H NMR (500 MHz, DMSO-d_6, δ ppm): 3.4351 (s, 1H, azetidin-2-one), 6.9455-6.9809 (ddd, 1H, *J* = 1.15, 4.75, 7.3 Hz, Ar-H), 6.9960-7.0311 (ddd, 1H, *J* = 0.65, 0.7, 5.55 Hz, Ar-H), 7.4095-7.4440 (dd, 1H, *J* = 1.75, 7.3 Hz, Ar-H), 7.6954-7.8076 (dd, 1H, *J* = 1.6, 7.7 Hz, Ar-H), 9.1748 (s, 1H, triazole), 9.1802 (s, 1H, triazole), 10.5057 (s, 1H, OH); ^{13}C NMR (100 MHz, DMSO-d_6, δ ppm): 46.02 (C-Cl), 62.63 (CH, azetidinone), 117.92-125.48 (Ar-C), 145.48, 146.88 (triazole), 157.94 (C-OH), 169.54 (C=O); MS (ESI): *m/z*: 265.20 $[M]^+$.

3-Chloro-4-(3-nitrophenyl)-1-(4*H*-1,2,4-triazol-4-yl)-azetidine-2-one (A4): Yield: 43.4%; m.p. 200-202 ºC; Elemental anal. of $C_{11}H_8ClN_5O_3$: calcd. (found) %: C, 44.99 (44.96); H, 2.75 (2.77); Cl, 12.07 (12.05); N, 23.85 (23.86); O, 16.34 (16.36); IR (KBr, ν_{max}, cm^{-1}): 1737.81 (C=O), 1348.92 (C-N, 3º amine), 1520.82, 1287.47 (NO_2), 888.03 (C-N, NO_2), 734.42 (C-Cl); ^{1}H NMR (500 MHz, DMSO-d_6, δ ppm): 3.4520 (s, 1H, azetidin-2-one), 7.8045-7.8921 (dd, 1H, *J* = 7.95, 7.95 Hz, Ar-H), 8.2633-8.3612 (td, 1H, *J* = 1.25, 2.55, 7.75 Hz, Ar-H), 8.4174-8.4778 (m, 1H, *J* = 1.35 Hz, Ar-H), 8.6158-8.6427 (tt, 1H, *J* = 1.9, 1.95, 9.6 Hz, Ar-H), 9.2152 (s, 1H, triazole), 9.2905 (s, 1H, triazole); ^{13}C NMR (100 MHz, DMSO-d_6, δ ppm): 49.90 (C-Cl), 63.81 (CH, azetidinone), 109.11-116.06 (Ar-C), 145.52, 148.59 (Ar-C), 147.25, 147.96 (triazole), 168.37 (C=O); MS (ESI): *m/z*: 293.95 $[M]^+$.

3-Chloro-4-(2,4-dichlorophenyl)-1-(4*H*-1,2,4-triazol-4-yl)azetidine-2-one (A5): Yield: 36%; m.p. 140-142 ºC; Elemental anal. of $C_{11}H_7Cl_3N_4O$: calcd. (found) %: C, 41.60 (41.62); H, 2.22 (2.25); Cl, 33.49 (33.45); N, 17.64 (17.64); O, 5.04 (5.04); IR (KBr, ν_{max}, cm^{-1}): 1718.74 (C=O), 1379.03 (C-N), 792.33, 717.65 (C-Cl); ^{1}H NMR (500 MHz, DMSO-d_6, δ ppm): 3.0780 (s, 1H, CH, azetidin-2-one), 7.6060-7.6272 (dd, 1H, *J* = 2.1, 2.05 Hz, Ar-H), 7.8399-7.8440 (d, 1H, *J* = 2.05 Hz, Ar-H), 8.0548-8.0719 (d, 1H, *J* = 8.55 Hz, Ar-H), 9.1880 (s, 1H, triazole), 9.2678 (s, 1H, triazole); ^{13}C NMR (100 MHz, DMSO-d_6, δ ppm): 50.04 (C-Cl), 60.41 (CH, azetidinone), 121.17-139.55 (Ar-C), 143.69, 144.53 (triazole), 169.25 (C=O); MS (ESI): *m/z*: 316.85 $[M]^+$.

3-Chloro-4-(4-hydroxy-3,5-dimethoxyphenyl)-1-(4*H*-1,2,4-triazol-4-yl)azetidine-2-one (A6): Yield: 50%; m.p. 215-217 ºC; Elemental anal. of $C_{13}H_{13}ClN_4O_4$: calcd. (found) %: C, 48.08 (48.05); H, 4.04 (4.04); Cl, 10.92 (10.93); N, 17.25 (17.26); O, 19.71 (19.72); IR (KBr, ν_{max}, cm^{-1}): 3675.92 (O-H), 2929.57 (C-H, CH_3-O), 1732.05 (C=O), 1327.89 (C-N), 1216.24 (C-O), 1470.43.60 (C-H *def.*), 1251.32, 1053.97 (C-O, Ar-O-CH_3), 783.93 (C-Cl); ^{1}H NMR (500 MHz, DMSO-d_6, δ ppm): 3.6193 (s, 1H, CH, azetidin-2-one), 3.8406, 3.8447 (s, 3H, -OCH_3), 7.1563, 7.2120 (s, 2H, Ar-H), 9.3276 (s, 2H, triazole), 9.7803 (s, 1H, -OH); ^{13}C NMR (100 MHz, DMSO-d_6, δ ppm): 48.52 (C-Cl), 56.90 (2C, -OCH_3), 62.37 (CH, azetidinone), 109.11-148.59 (Ar-C), 145.52, 147.25 (triazole), 174.23 (C=O); MS (ESI): *m/z*: 324.11 $[M]^+$.

3-Chloro-4-(1*H*-indol-3-yl)-1-(4*H*-1,2,4-triazol-4-yl)-azetidine-2-one (A7): Yield: 18.8%; m.p. 160-161 ºC; Elemental anal. of $C_{13}H_{10}ClN_5O$: calcd. (found) %: C, 54.27 (54.27); H, 3.50 (3.52); Cl, 12.32 (12.31); N, 24.34 (24.34); O, 5.57 (5.56); IR (KBr, ν_{max}, cm^{-1}): 1714.25 (C=O), 1567.90 (N-H *def.*); 1390.28 (C-N, 3º amine), 1327.52 (C-N, 2º amine), 754.47 (C-Cl); ^{1}H NMR (500 MHz, DMSO-d_6, δ ppm): 3.4356 (s, 1H, azetidin-2-one), 7.2201-7.2941 (ddd, 2H, *J* = 1.15, 7.2, 28.65 Hz, indole), 7.5275-7.5448 (dd, 1H, 6.75, 0.8 Hz, indole), 8.1185-8.1339 (d, 1H, *J* = 7.7Hz, indole), 8.2915-8.2978 (d, 1H, *J* = 3.15Hz, indole), 9.9621 (s, 2H, triazole), 12.1577 (s, 1H, NH, pyrrole); ^{13}C NMR (100 MHz, DMSO-d_6, δ ppm): 47.52 (C-Cl), 54.30 (CH, azetidinone), 112.93-139.41 (indole C), 150.43, 151.18 (triazole), 166.51 (C=O); MS (ESI): *m/z*: 288.14 $[M]^+$.

3-Chloro-4-(4-dimethylamino)phenyl)-1-(4*H*-1,2,4-triazol-4-yl)azetidine-2-one (A8): Yield: 46%; m.p.: 52-53 ºC; Elemental anal. of $C_{13}H_{14}ClN_5O$: calcd. (found) %: C, 53.52 (53.55); H, 4.84 (4.83); Cl, 12.15 (12.14); N, 24.01 (24.00); O, 5.48 (5.48); IR (KBr, ν_{max}, cm^{-1}): 2982.40 (C-H), 1716.10 (C=O), 1433.83 (C-H *def.*); 1345.01 (C-N), 777.86 (C-Cl); ^{1}H NMR (500 MHz, DMSO-d_6, δ ppm): 3.0951 (s, 6H, -CH_3), 3.5892 (s, 1H, azetidin-2-one), 6.7221-6.7221 (dd, 2H, *J* = 7.6, 12.4 Hz, Ar-H), 7.4948-7.5194 (d, 2H, *J* = 7.6Hz, Ar-H), 8.7428 (s, 2H, triazole); ^{13}C NMR (100 MHz, DMSO-d_6, δ ppm): 36.08 (2C, -CH_3), 45.47 (C-Cl), 55.72 (CH, azetidinone), 112.70-143.89 (Ar-C), 155.13, 155.96 (triazole), 170.42 (C=O); MS (ESI): *m/z*: 292.08 $[M]^+$.

3-Chloro-4-(2,4-dimethoxyphenyl)-1-(4*H*-1,2,4-triazol-4-yl)azetidine-2-one (A9): Yield: 42%; m.p.: 50-51 ºC; Elemental anal. of $C_{13}H_{13}ClN_4O_3$: calcd. (found) %: C, 50.58 (50.58); H, 4.24 (4.20); Cl, 11.48 (11.49); N, 18.15 (18.16); O, 15.55 (15.57); IR (KBr, ν_{max}, cm^{-1}): 2868.65 (C-H, CH_3-O), 1725.55 (C=O), 1473.02 (C-H *def.*), 1323.85 (C-N), 1257.82, 1012.04 (C-O, Ar-O-CH_3), 730.37 (C-Cl); ^{1}H NMR (500 MHz, $CDCl_3$): 3.7091-3.7154 (s, 6H, -CH_3), 4.2127 (s, 1H, azetidin-2-one), 7.3920 - 7.4136 (dd, 1H, *J* = 0.3, 8.5Hz, Ar-H), 7.5191-7.5231 (d, 1H, *J* = 2.0 Hz, Ar-H), 8.0927-8.1099 (d, 1H, *J* = 8.55Hz, Ar-H), 8.7254 (s, 2H, triazole); ^{13}C NMR (100 MHz, DMSO-d_6, δ ppm): 46.48 (C-Cl), 55.28, 55.40 (-OCH_3), 57.09 (CH, azetidinone), 108.42-162.27 (Ar-C), 153.88, 154.40 (triazole), 168.91 (C=O); MS (ESI): *m/z*: 309.10 $[M]^+$.

3-Chloro-4-(3-ethoxy-4-hydroxyphenyl)-1-(4*H*-1,2,4-triazol-4-yl)azetidine-2-one (A11): Yield: 47%; m.p.: 90-91 ºC; Elemental anal. of $C_{13}H_{13}ClN_4O_3$: calcd. (found) %: C, 50.58 (50.55); H, 4.24 (4.25); Cl, 11.48 (11.47); N, 18.15 (18.16); O 15.55 (15.57); IR (KBr, ν_{max}, cm^{-1}): 3624.95 (O-H), 2924.38 (-CH_2), 1730.82 (C=O), 1469.12 (-CH_2 *def.*), 1424.78 (-CH_3 *def.*), 1301.97 (C-N), 1246.10, 1051.77 (C-O, Ar-O-CH_3), 1166.74 (C-O), 751.56 (C-Cl); ^{1}H NMR (500 MHz, DMSO-d_6, δ ppm): 1.20 (t, 3H, -CH_3), 3.8359 (s, 1H, azetidine-2-one), 4.1637 (q, 2H, -CH_2), 7.1258-7.1489 (dd, 2H, *J* = 2.0, 2.7Hz, Ar-H), 7.8420-7.8710 (ddd, 2H, *J* = 2.9, 5.0, 2.75Hz, Ar-H), 9.1345 (s, 1H, -OH), 9.5233, 9.5336 (s, 2H, triazole); ^{13}C NMR (100 MHz, DMSO-d_6, δ ppm): 17.59 (-CH_3), 45.40 (C-Cl), 55.88 (CH, azetidinone), 72.94, 73.32 (-CH_2), 101.72-155.77 (Ar-C), 150.57, 151.82 (triazole), 169.83 (C=O); MS (ESI): *m/z*: 309.08 $[M]^+$.

3-Chloro-4-(4-hydroxyphenyl)-1-(4*H*-1,2,4-triazol-4-yl)azetidine-2-one (A12): Yield: 38%; m.p.: 220-221 ºC, Elemental anal. of $C_{11}H_9ClN_4O_2$: calcd. (found) %: C, 49.92 (49.95); H 3.43 (3.43); Cl, 13.40 (13.38); N, 21.17 (21.14); O, 12.08 (12.10); IR (KBr, ν_{max}, cm^{-1}): 3611.80 (O-H), 1705.78 (C=O), 1386.67 (O-H *def.*), 1340.22 (C-N), 1213.64 (C-O), 748.68 (C-Cl); ^{1}H NMR (500 MHz, DMSO-d_6, δ ppm): 3.3757 (s, 1H, CH, azetidine-2-one), 8.0946-8.1123 (d, 2H, *J* = 8.85 Hz, Ar-H), 8.3955-8.4131 (d, 2H, *J* = 8.8, Ar-H), 9.2067 (s, 2H, triazole), 9.2544 (s, 1H, -OH); ^{13}C NMR (100 MHz, DMSO-d_6, δ ppm): 43.97 (C-Cl), 62.32 (CH, azetidinone), 115.30-158.75 (Ar-C), 156.04, 156.36 (triazole), 164.61 (C=O); MS (ESI): *m/z*: 265.13 $[M]^+$.

***In vitro* antitubercular activity on *Mtb* H37Rv:** Antitubercular activity was evaluated against *M. tuberculosis* H37Rv using the broth dilution method. The minimum inhibitory concentration (MIC) of each compound was determined over a concentration range of 1000-7.81 μg/mL following the standard procedure [44-46]. All experiments were performed in duplicate using microtiter plates. The MIC was defined as the lowest concentration that inhibited ≥ 99% of bacterial growth. Rifampicin (1 μg/mL) and isoniazid (0.25 μg/mL) were used as reference drugs.

***In vitro* cell viability studies:** The *in vitro* cytotoxicity of the synthesized compounds was evaluated using the MTT assay in Vero cell lines according to the standard procedure [47-49].

***In vivo* acute toxicity studies:** The acute oral toxicity of the synthesised compounds was evaluated in accordance with OECD Guideline 423 [50]. The study was conducted in a stepwise manner, with each step consisting of three albino mice of the same sex along with a control group. All animals were weighed prior to dosing. Compounds that exhibited notable anti-tubercular activity were administered orally at doses of 2000 and 300 mg/kg body weight, suspended in a 1% CMC solution. Post-administration, the animals were closely monitored for behavioural alterations such as nervousness, hyperactivity, lethargy and loss of coordination, as well as for signs of mortality. Special attention was given to the initial 4 h post-dosing, following which the animals were monitored daily for 14 days to observe for any signs of acute toxicity. At the end of the observation period, the mice were humanely killed and their major organs, such as the heart, liver and kidneys, were taken for histopathological studies [51-53].

RESULTS AND DISCUSSION

A series of triazolyl-substituted azetidinone derivatives were synthesised *via* a two-step reaction sequence. Initially, Schiff bases were synthesised by condensing equimolar amounts of 4-amino-1,2,4-triazole (**1**) with substituted aromatic aldehydes in methanol using a catalytic quantity of glacial acetic acid. The resulting imines (**T1-T12**) were subjected to cyclocondensation with chloroacetyl chloride in the presence of triethylamine as base in dry dioxane to afford the corresponding 2-azetidinone derivatives (**A1-A12**) (**Scheme-I**).

Homology modelling: In this work, 14 significant homologous sequences were identified. Among these, PDB entries 5LLB_C, 5LL0_A, 4YEG_A and 5LLF_A exhibited the highest similarity, each with 83% query coverage and 53.88% sequence identity, whereas the remaining 10 sequences showed less than 50% sequence identity. PDB entry 5LLB_C, corresponding to polyphosphate kinase 2 (PPK2) from *Francisella tularensis* complexed with $AMPPCH_2PPP$ and polyphosphate, was selected as the template since it contained only 18 unaligned residues at the N-terminus and a single unaligned residue at the C-terminus.

The quality of the modelled structure was evaluated using the PROCHECK web server. Ramachandran plot analysis placed 91.5% of the residues in the most favoured regions, 7.0% in the additionally allowed regions, 0.9% in the generously allowed regions and 0.5% in the disallowed regions, which confirmed the good stereochemical quality of the model. Structural stability was assessed by molecular dynamics (MD) simulations using Schrödinger Desmond. Prior to root mean square deviation (RMSD) analysis, all trajectory frames were aligned to the backbone atoms of the reference structure. The RMSD profile of the modelled protein is presented in Fig. 2 (*y*-axis). RMSD values remained within the acceptable range of 1-3 Å throughout the simulation, which indicate that the modelled structure retained its conformational stability without significant structural deviations.

Molecular docking: Molecular docking against the crystal structure of PPK2 from *F. tularensis* (PDB ID: 5LLB_C) identified several synthesised compounds with favourable binding affinities relative to the reference drugs. Streptomycin exhibited the highest docking score (-8.12 kcal/mol), although no specific residue interactions were observed,

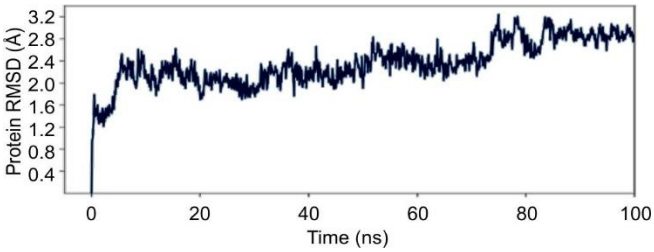

Fig. 2. Modeled protein RMSD by MD simulation

implying binding through non-classical contacts. Among the synthesised compounds, **A8** (-7.73 kcal/mol), **T7** (-7.59 kcal/mol) and A7 (-7.29 kcal/mol) displayed strong binding affinities with interactions involving the key residues LYS165, ILE194 and PHE149. Compound **A11** formed multiple interactions with SER20, ILE21, GLY192 and ILE194, consistent with stable ligand binding. Residues ILE194 and LYS165 were common interaction sites for the most active compounds, suggesting their possible role in PPK2 inhibition. The reference drugs isoniazid and bedaquiline exhibited lower docking scores of -5.85 and -4.43 kcal/mol, respectively, than the most active synthesised compounds (Table-2).

Docking studies performed with the homology-modelled PPK2 protein of *M. tuberculosis* yielded comparable results.

TABLE-2
DOCKING SCORE AND INTERACTIONS OF LIGANDS ON 5LLB_C PROTEIN AND PPK2 MODELED PROTEIN

Compd.	5LLB_C Protein interactions			Compd.	PPK2 Modeled protein interactions		
	Docking score (kcal/mol)	Glide energy (kcal/mol)	Interactions		Docking score (kcal/mol)	Glide energy (kcal/mol)	Interactions
A_8	-5.97	-31.38	LYS89	**A_{12}**	-6.01	-29.48	ASN131, GLU136
T_7	-5.90	-29.80	ASN122	**A_{11}**	-5.76	-31.89	ASN131, GLU136, PHE141
A_7	-5.77	-34.40	ARG118, ASN122	**T_6**	-5.64	-29.43	ASN131, GLU136
A_3	-5.53	-30.66	LYS89, ASN122	**A_2**	-5.61	-30.37	ASN131, GLU136, PHE141
A_1	-5.44	-32.92	LYS89, GLU127	**T_{12}**	-5.55	-24.97	ASN131, GLU136, PHE141
Isoniazid	-5.42	-23.17	LEU87, ASN122	**A_6**	-5.53	-31.81	ASN131, GLU136, PHE141
T_1	-5.41	-33.52	ALA63, ARG118, ARG178	**A_3**	-4.98	-35.59	GLY72, LYS75, ASP126, ARG127, ARG187, LYS196, LYS196
T_4	-5.36	-33.32	ALA63, ARG118, ARG178	**T_{11}**	-4.93	-29.73	ASN131, GLU136
A_{12}	-5.25	-30.75	ARG118, ASN122	**T_4**	-4.88	-29.05	ASN131, ARG132, GLU136, PHE141
T_8	-5.24	-29.58	ARG95	**T_5**	-4.85	-30.89	GLY72, LYS75, ARG187
A_2	-5.08	-33.27	ARG118, ASN122	**A_8**	-4.68	-27.37	No interactions
A_{11}	-5.04	-34.55	ARG118, ASN122	**T_1**	-4.67	-29.85	GLY72, LYS75, ARG187
A_4	-4.93	-31.52	LYS89, PHE132	Isoniazid	-4.57	-22.11	LYS75, ASP126, ARG127, ARG187
T_{11}	-4.92	-30.86	ARG118, ASN122	**T_8**	-4.56	-24.18	ASN131, PHE141
A_9	-4.90	-30.20	LYS89	**A_7**	-4.55	-34.68	GLY72, LYS75, LYS75, ASP126, ARG127, ARG187
T_5	-4.89	-31.11	ALA63, LYS66, ARG118, ARG178	**T_2**	-4.54	-33.64	LEU96, LYS75, ARG187
T_3	-4.88	-28.85	ASP62, ALA63, LYS66, ARG178	**A_{10}**	-4.46	-25.49	ARG104
T_{10}	-4.81	-28.61	ARG95	**T_{10}**	-4.35	-23.69	PHE141
T_9	-4.79	-29.86	ARG95, PHE132	**T_7**	-4.30	-32.30	LYS75, GLY76, LEU96, ARG187
A_6	-4.78	-33.16	ARG118, ASN122	**A_4**	-4.12	-33.05	LYS75, ASP126, ARG127, ARG187, ARG187, LYS196
T_2	-4.77	-32.17	LYS66, LEU87, ARG178	**T_3**	-4.12	-31.45	GLY74, LYS75, GLY76, ARG127, ARG187, ASP201
T_{12}	-4.67	-27.85	ARG95	**A_9**	-3.85	-33.66	LYS75, ARG127, ARG187, ARG187, LYS196
T_6	-4.62	-27.95	PHE132	**T_9**	-3.74	-29.34	LYS75, ARG187
A_{10}	-4.45	-31.93	No interactions	**A_1**	-3.67	-28.80	GLY72, LYS75, LYS196, ARG127
A_5	-4.09	-31.41	ARG102, ARG118	**A_5**	-3.60	-29.17	GLY72, LYS75, ARG187, LYS196, LYS196
Bedaquiline	-3.56	-39.67	ASN122	Bedaquiline	-3.29	-36.00	LYS75, LEU96

Black: H-bond; Red: Pi-cation; Green: Pi-Pi stacking; Gold: Halogen bond; Blue: Salt bridge

Streptomycin achieved the highest binding affinity (-6.01 kcal/mol), forming interactions with ASP71, LYS75, ASP126, ARG127 and LYS196. Compound **A12** exhibited the same docking score (-6.01 kcal/mol) and formed hydrogen bonds with ASN131 and GLU136. Compounds **A11** (-5.76 kcal/mol) and **A2** (-5.61 kcal/mol) interacted with ASN131, GLU136 and PHE141. **T4** (-4.88 kcal/mol) and **T5** (-4.85 kcal/mol) established contacts with ASN131, ARG132, PHE141 and GLY72, whereas **A3** (-4.98 kcal/mol) and **A7** (-4.55 kcal/ mol) interacted with GLY72, LYS75, ASP126, ARG127, ARG187 and LYS196. Isoniazid (-4.57 kcal/mol) interacted with LYS75, ASP126, ARG127 and ARG187, while bedaquiline (-3.29 kcal/ mol) formed contacts with LYS75 and LEU96. The favourable docking scores and interactions observed for compounds **A11** and **A12** with residues LYS75, ASN131, GLU136 and ARG127 support their selection for further investigation as potential PPK2 inhibitors. The 2D binding interaction images of **A11**, **A12**, isoniazid and bedaquiline with the modelled PPK2 protein are shown in Fig. 3.

Heatmap of residue interaction frequencies: The interaction heatmap summarizes the frequency of amino acid contacts formed by the docked compounds with the 5LLB_C protein. ARG118 and ASN122 were the most frequently contacted residues, with 11 and 9 interactions, respectively, followed by ARG178 (6), LYS89 (5) and ARG95 (4), identifying these residues as the principal binding-site hotspots. PHE132, LYS66, LEU87 and ALA63 exhibited fewer contacts and contributed to ligand stabilization. The heatmap of the modelled PPK2 protein identified LYS75 (16 interactions) and ARG187 (14 interactions) as the predominant binding hotspots, followed by ASN131 (9), GLU136 (8) and ARG127 (8) (Fig. 4).

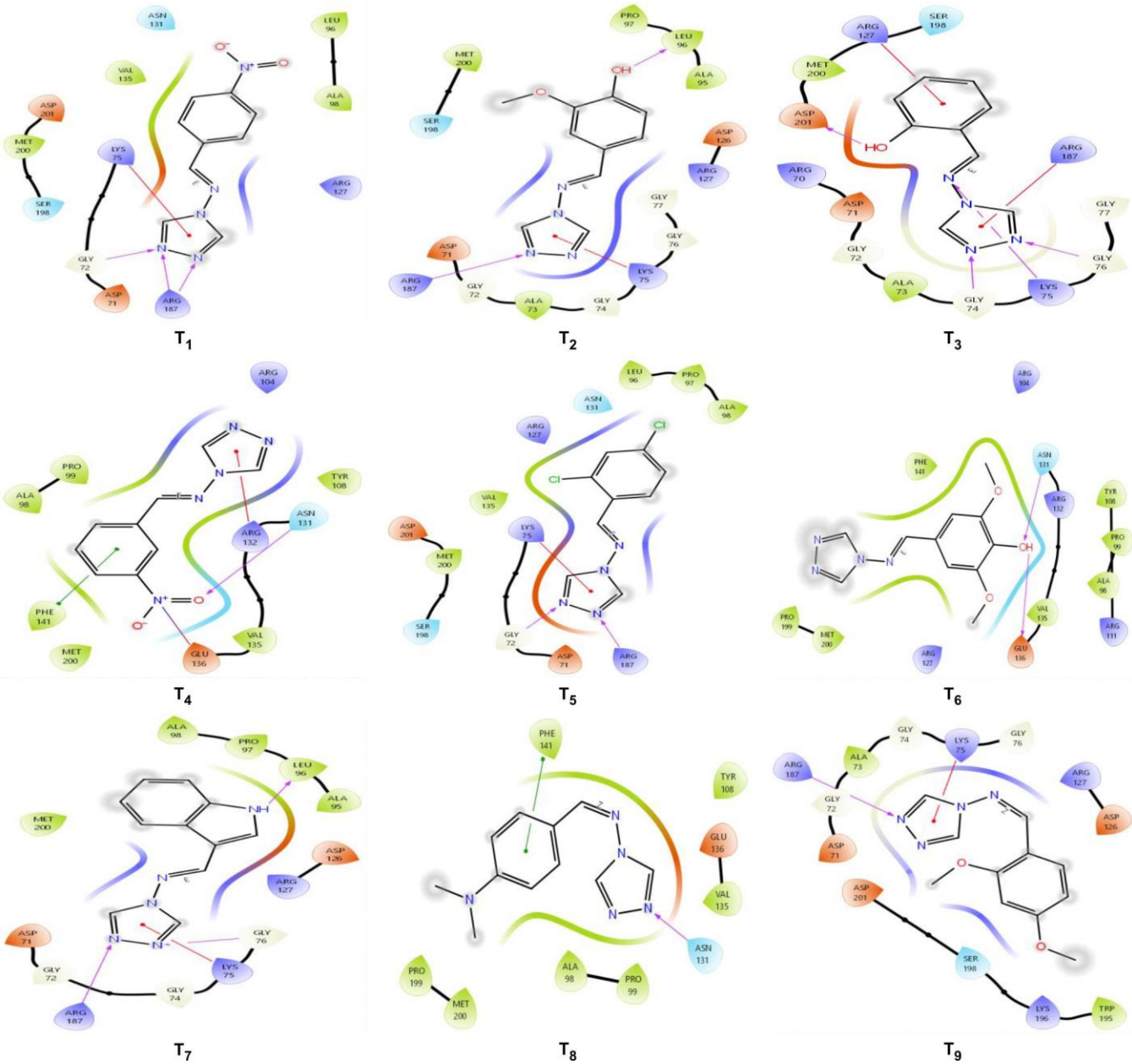

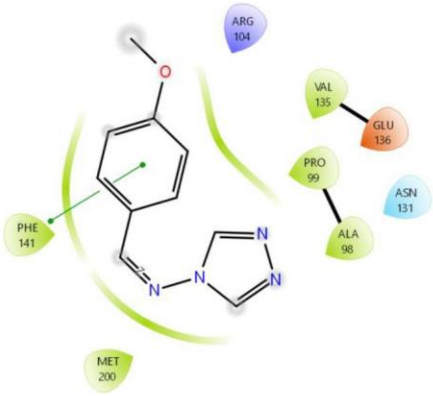

T_{10}

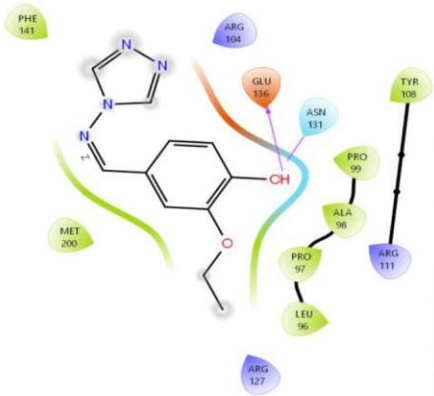

T_{11}

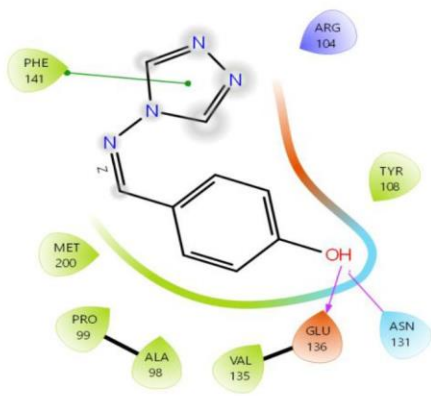

T_{12}

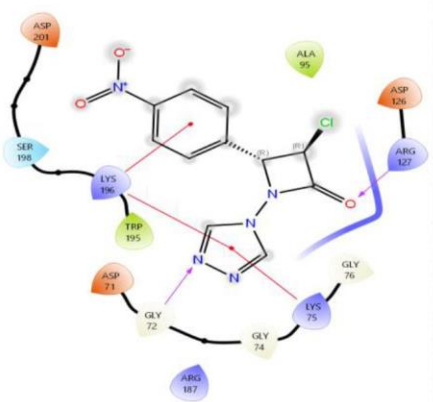

A_1

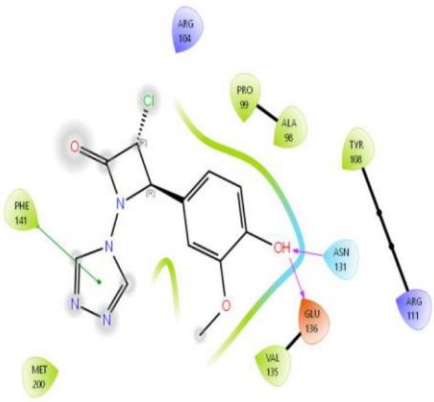

A_2

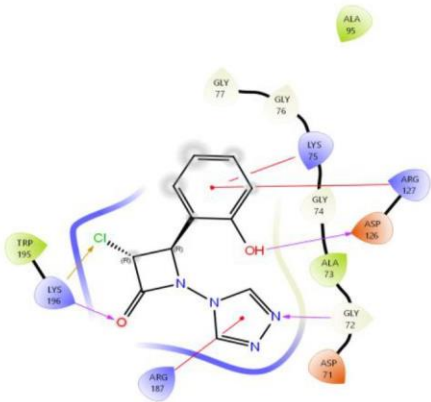

A_3

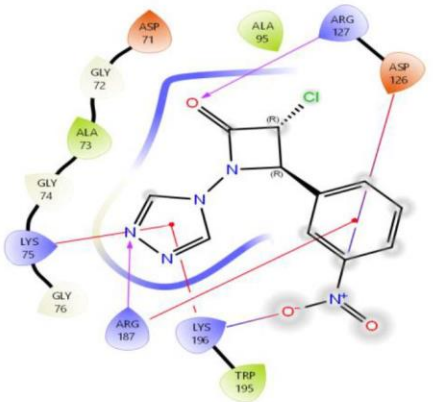

A_4

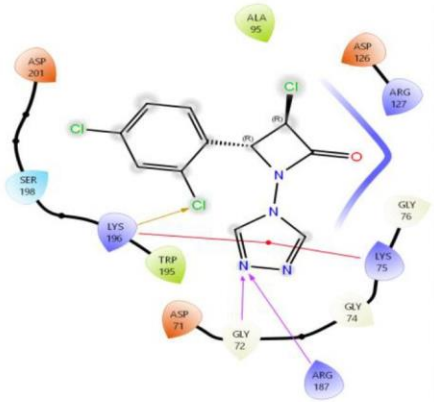

A_5

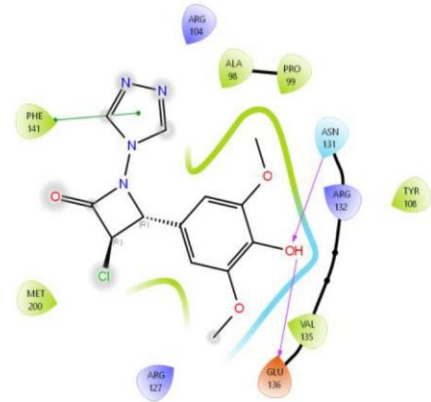

A_6

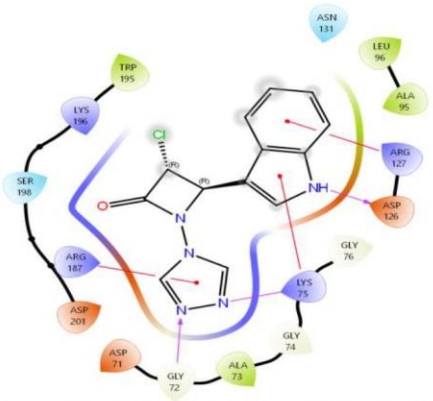

A_7

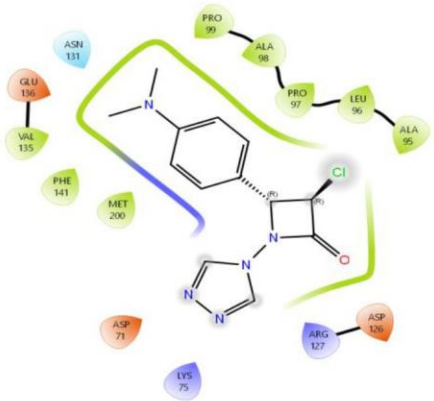

A_8

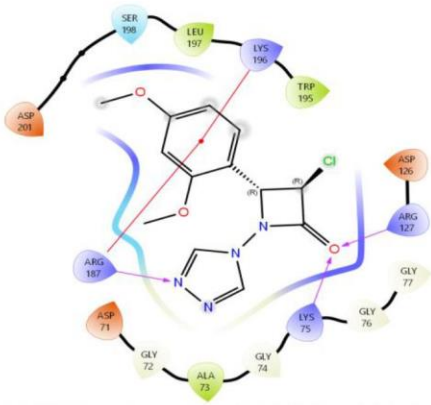

A_9

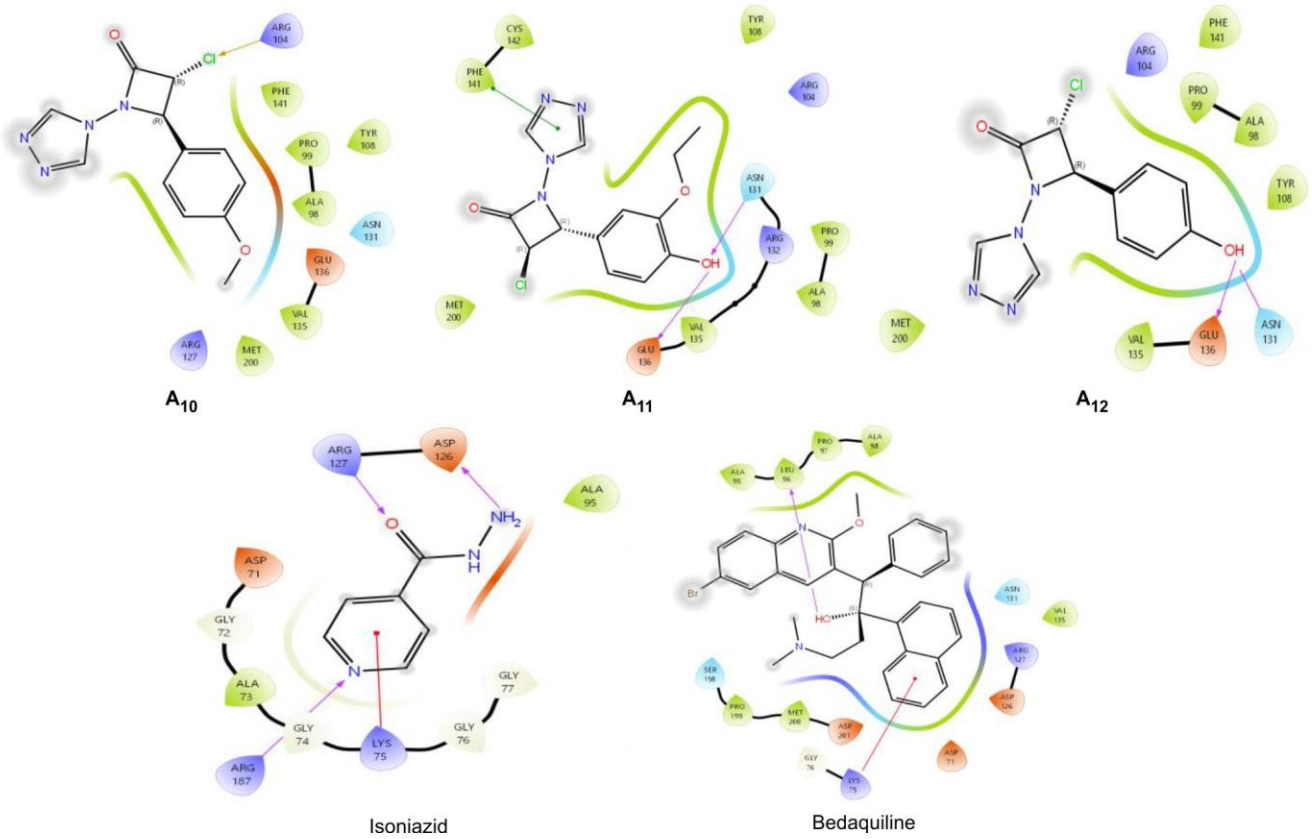

Fig. 3. 2D interactions of the compounds **T1-12**, **A1-12**, isoniazid and bedaquiline against modeled protein of PPK2

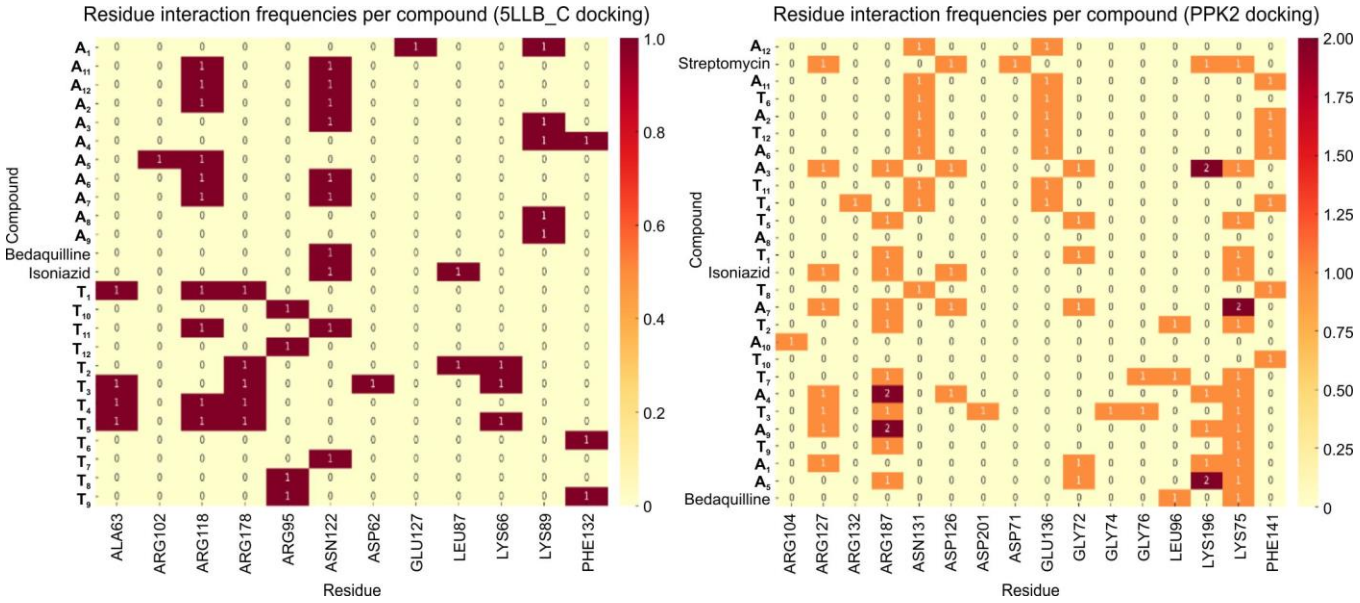

Fig. 4. Heatmap of residue interaction frequencies on 5LLB_C and PPK2 modeled protein

ADMET studies: The physico-chemical and medicinal properties of the synthesised triazoles **T1-T12** and azetidinone (**A1-A12**) derivatives were evaluated to assess their drug-likeness and all compounds satisfied Lipinski's rule of five, supporting their suitability as orally active drug candidates (Table-3). The molecular weights of the triazole derivatives ranged from 188.07 to 248.09 g/mol, whereas those of the azetidinone derivatives ranged from 264.04 to 324.06 g/mol, remaining well within the acceptable range for favourable absorption and permeability. The number of hydrogen bond acceptors (4-8) and hydrogen bond donors (0-1), together with topological polar surface area (TPSA) values of 43.07-94.16 Å^2, reflected a balanced hydrophilic-lipophilic profile that favours receptor interactions and membrane diffusion. The low number of rotatable bonds (≤ 4) corresponds to relatively rigid molecular frameworks, a characteristic often asso-

TABLE-3
PHYSICO-CHEMICAL PROPERTIES OF SYNTHESISED COMPOUNDS (T_1-T_{12}) AND (A_1-A_{12})

Compd.	MW	Volume	Density	nHA	nHD	TPSA	nROT	Synthetic accessibility score	Lipinski	LogS	LogD	Logp
T_1	217.06	201.216	1.079	7	0	86.21	3	2.512	Accepted	-3.345	1.544	1.662
T_2	218.08	210.152	1.038	6	1	72.53	3	2.53	Accepted	-1.555	0.343	-0.151
T_3	188.07	184.066	1.022	5	1	63.3	2	2.621	Accepted	-1.376	0.723	0.466
T_4	217.06	201.216	1.079	7	0	86.21	3	2.564	Accepted	-3.268	1.529	1.595
T_5	240.00	205.698	1.167	4	0	43.07	2	2.594	Accepted	-3.788	2.587	2.934
T_6	248.09	236.238	1.050	7	1	81.76	4	2.572	Accepted	-1.625	0.377	-0.141
T_7	211.09	209.672	1.007	5	1	58.86	2	2.698	Accepted	-2.189	1.001	0.96
T_8	215.12	220.864	0.974	5	0	46.31	3	2.514	Accepted	-2.383	1.654	1.574
T_9	232.10	227.448	1.020	6	0	61.53	4	2.446	Accepted	-2.532	1.645	1.653
T_{10}	202.09	201.362	1.004	5	0	52.3	3	2.326	Accepted	-2.404	1.414	1.515
T_{11}	232.10	227.448	1.020	6	1	72.53	4	2.549	Accepted	-1.719	0.866	0.401
T_{12}	188.07	184.066	1.022	5	1	63.3	2	2.531	Accepted	-1.537	0.32	-0.079
A_1	293.03	251.253	1.166	8	0	94.16	3	3.682	Accepted	-3.175	2.094	1.14
A_2	294.05	260.189	1.130	7	1	80.48	3	3.718	Accepted	-2.41	1.29	0.281
A_3	264.04	234.103	1.128	6	1	71.25	2	3.74	Accepted	-2.24	1.278	0.505
A_4	293.03	251.253	1.166	8	0	94.16	3	3.734	Accepted	-3.038	2.101	1.149
A_5	315.97	255.735	1.236	5	0	51.02	2	3.738	Accepted	-3.374	3.058	2.55
A_6	324.06	286.275	1.132	8	1	89.71	4	3.743	Accepted	-2.795	1.272	0.168
A_7	287.06	259.708	1.105	6	1	66.81	2	3.739	Accepted	-3.152	1.873	1.276
A_8	291.09	270.901	1.075	6	0	54.26	3	3.684	Accepted	-2.504	1.887	1.217
A_9	308.07	277.485	1.110	7	0	69.48	4	3.595	Accepted	-2.915	1.892	1.11
A_{10}	278.06	251.399	1.106	6	0	60.25	3	3.539	Accepted	-2.792	1.799	1.141
A_{11}	308.07	277.485	1.110	7	1	80.48	4	3.718	Accepted	-2.689	1.909	0.926
A_{12}	264.04	234.103	1.128	6	1	71.25	2	3.723	Accepted	-2.354	1.344	0.426

ciated with enhanced binding affinity and conformational stability. The azetidinone derivatives possessed slightly higher molecular weights, TPSA values and lipophilicity than the corresponding triazole derivatives. These characteristics may contribute to improved membrane permeability and enhanced affinity toward biological targets.

The *in silico* ADME evaluation of the synthesised triazoles **T_1-T_{12}** and azetidinone (**A_1-A_{12}**) derivatives demonstrated favourable pharmacokinetic characteristics consistent with orally active drug candidates (Table-4). The predicted Caco-2 permeability values ranged from -5.17 to -4.49, corresponding to moderate-to-good intestinal permeability.

TABLE-4
ADME PROPERTIES OF COMPOUNDS (T_1-T_{12}) AND (A_1-A_{12})

Code	Caco-2	BBB	HIA	PPB (%)	VDss	CYP1A2-inh	CYP1A2-sub	CYP2C19-inh	CYP2C19-sub	CYP2C9-inh	CYP2C9-sub	CYP2D6-inh	CYP2D6-sub	CYP3A4-inh	CYP3A4-sub	CL	$T_{1/2}$
T_1	-4.63	0.147	0.007	64.60	0.935	0.987	0.184	0.790	0.069	0.620	0.230	0.026	0.057	0.053	0.215	9.310	0.856
T_2	-4.84	0.385	0.008	73.96	1.07	0.996	0.852	0.918	0.066	0.863	0.759	0.487	0.102	0.341	0.346	8.425	0.955
T_3	-4.85	0.339	0.015	57.77	0.996	0.996	0.517	0.946	0.066	0.884	0.759	0.476	0.043	0.244	0.322	8.794	0.961
T_4	-4.64	0.186	0.007	65.83	0.844	0.991	0.275	0.874	0.076	0.721	0.123	0.034	0.047	0.102	0.222	9.360	0.886
T_5	-4.49	0.033	0.004	94.50	1.786	0.994	0.480	0.966	0.192	0.874	0.151	0.055	0.031	0.107	0.430	10.45	0.598
T_6	-4.87	0.297	0.013	84.21	1.052	0.993	0.947	0.890	0.198	0.817	0.656	0.189	0.134	0.299	0.545	7.632	0.951
T_7	-4.78	0.540	0.011	77.69	1.233	0.997	0.508	0.969	0.072	0.902	0.621	0.537	0.052	0.524	0.322	7.376	0.956
T_8	-4.72	0.772	0.008	75.47	1.226	0.994	0.603	0.868	0.186	0.770	0.053	0.030	0.021	0.076	0.303	10.31	0.921
T_9	-4.67	0.579	0.007	74.65	1.383	0.992	0.921	0.912	0.646	0.630	0.181	0.042	0.034	0.167	0.488	10.06	0.902
T_{10}	-4.69	0.518	0.006	58.82	1.555	0.993	0.710	0.896	0.194	0.707	0.096	0.064	0.017	0.110	0.396	9.512	0.904
T_{11}	-4.86	0.224	0.006	77.26	0.986	0.995	0.638	0.946	0.068	0.907	0.755	0.439	0.073	0.305	0.375	7.621	0.942
T_{12}	-4.90	0.332	0.012	48.70	1.061	0.996	0.486	0.934	0.060	0.849	0.721	0.361	0.052	0.131	0.250	8.595	0.959
A_1	-4.79	0.113	0.005	54.74	0.804	0.635	0.889	0.243	0.161	0.138	0.095	0.032	0.051	0.124	0.639	9.505	0.867
A_2	-5.03	0.239	0.005	62.27	0.756	0.646	0.961	0.109	0.250	0.124	0.253	0.018	0.063	0.207	0.716	13.25	0.945
A_3	-5.16	0.193	0.005	53.93	0.674	0.726	0.881	0.127	0.168	0.139	0.361	0.026	0.049	0.140	0.621	12.46	0.955
A_4	-4.78	0.139	0.005	55.56	0.828	0.735	0.892	0.268	0.138	0.191	0.072	0.045	0.045	0.261	0.636	9.871	0.906
A_5	-4.59	0.031	0.004	91.93	1.073	0.940	0.868	0.644	0.569	0.352	0.082	0.041	0.034	0.507	0.844	8.981	0.743
A_6	-4.92	0.129	0.008	74.89	0.713	0.472	0.978	0.062	0.590	0.079	0.277	0.013	0.071	0.162	0.846	12.57	0.933
A_7	-4.63	0.220	0.004	68.33	0.871	0.938	0.884	0.357	0.271	0.288	0.168	0.054	0.046	0.489	0.651	10.51	0.941
A_8	-4.74	0.775	0.006	72.74	1.235	0.846	0.928	0.286	0.674	0.263	0.057	0.018	0.065	0.146	0.733	11.42	0.921
A_9	-4.75	0.432	0.005	73.70	0.905	0.878	0.967	0.342	0.800	0.165	0.150	0.019	0.085	0.258	0.851	11.27	0.921
A_{10}	-4.76	0.547	0.004	56.10	1.027	0.776	0.933	0.388	0.692	0.182	0.102	0.029	0.062	0.245	0.749	11.57	0.909
A_{11}	-5.07	0.070	0.004	66.54	0.669	0.871	0.903	0.214	0.261	0.311	0.292	0.024	0.051	0.288	0.717	11.99	0.920
A_{12}	-5.17	0.235	0.005	50.49	0.769	0.586	0.882	0.126	0.090	0.088	0.168	0.017	0.046	0.071	0.543	13.26	0.952

Human intestinal absorption exceeded 50% for most compounds, supporting efficient gastrointestinal uptake. Plasma protein binding values ranged from 50% to 95%, favouring prolonged systemic exposure and an extended circulation half-life. The predicted steady-state volume of distribution (VDss) varied between 0.67 and 1.78 L/kg, reflecting moderate tissue distribution, with compounds **T5** and **A8** exhibiting comparatively higher distribution values. Cytochrome P450 interaction analysis identified most compounds as substrates or moderate inhibitors of CYP1A2, CYP2C19, CYP2C9 and CYP3A4 isoforms. These observations identify metabolic pathways that could be considered during structural optimisation to minimise potential drug-drug interactions. Clearance values ranged from 0.215 to 0.851 mL/min/kg, while the predicted elimination half-lives varied from 7.3 to 13.3 h, reflecting a favourable balance between metabolic stability and elimination, which may support satisfactory bioavailability and convenient dosing intervals.

Compounds **A2**, **A3**, **A6** and **A12** exhibited predicted elimination half-lives exceeding 12 h, consistent with greater metabolic stability. Compounds **T5** and **T8** exhibited comparatively lower predicted clearance, favouring prolonged systemic retention. These pharmacokinetic characteristics provide a useful basis for selecting candidates for further preclinical optimisation. The *in silico* toxicity assessment of the synthesised triazolylazetidinone derivatives revealed a favourable safety profile with low predicted risks of cardiotoxicity and bioaccumulation, moderate risks of genotoxicity and hepatotoxicity and manageable risks associated with metabolism and environmental toxicity (Table-5). These findings support the continued development of these compounds as lead structures, while structural optimisation may further improve their safety margins during subsequent stages of drug development.

Antitubercular activity: *in vitro* method: The synthesised compounds (**A1-A12**) were evaluated for antitubercular activity against the *Mtb* H37Rv strain using the minimum inhibitory concentration (MIC) method. The MIC was defined as the lowest concentration required to inhibit 99.9% of bacterial growth and the results are shown in Table-6. Among the tested derivatives, **A11** and **A12** exhibited the highest activity, with MIC values ≤ 7.81 μg/mL. Compounds **A1** and **A7** showed MIC values of 15.62 μg/mL, followed by **A4** (62.5 μg/mL), **A3** and **A6** (125 μg/mL), **A2** and A8 (250 μg/mL), **A9** and **A10** (500 μg/mL) and **A5** (1000 μg/mL), representing varying degrees of antitubercular activity. The marked variation in MIC values across the series reflects the influence of structural modifications on antitubercular potency. Fluorescence micrographs of **A1**, **A11** and **A12** are shown in Fig. 5.

***In vitro* cell-line toxicity:** Cytotoxicity investigation of the synthesised compounds **A1**, **A4**, **A7**, **A11** and **A12** was performed on Vero cells [33] and it was found that there was a dose-dependent decrease in viability of cells over the concentration range (3.125-100 μg/mL), as shown in Table-7. At the highest tested concentration (100 μg/mL), cell viability decreased markedly, whereas nearly 100% viability was retained at 3.125 μg/mL. The calculated IC_{50} values were consistent with this concentration-dependent cytotoxic response. Among the tested compounds, **A11** exhibited the highest cytotoxicity, with the lowest IC_{50} value (11.75 μg/mL), followed

TABLE-5
TOXICITY PARAMETERS OF COMPOUNDS (**T1-T12**) AND (**A1-A12**)

Compd.	Herg blocker	DILI	ROA	Ame's mutagenicity	Skin sensitisation	FDAMDD	EI	Carcinogenecity	Hepatotoxicity	Respiratory	BCF
T1	0.002	0.974	0.399	0.970	0.803	0.032	0.979	0.853	0.780	0.765	0.501
T2	0.013	0.950	0.718	0.972	0.127	0.078	0.827	0.972	0.789	0.951	0.629
T3	0.005	0.969	0.780	0.978	0.627	0.029	0.943	0.964	0.705	0.951	0.592
T4	0.003	0.970	0.505	0.959	0.795	0.051	0.975	0.876	0.814	0.763	0.468
T5	0.001	0.976	0.151	0.762	0.709	0.093	0.922	0.803	0.233	0.693	1.334
T6	0.040	0.937	0.526	0.952	0.083	0.043	0.460	0.980	0.818	0.954	0.465
T7	0.011	0.978	0.977	0.986	0.587	0.763	0.768	0.903	0.844	0.972	0.454
T8	0.018	0.968	0.502	0.963	0.737	0.060	0.955	0.896	0.303	0.953	0.602
T9	0.012	0.945	0.566	0.953	0.268	0.125	0.857	0.954	0.700	0.933	0.752
T10	0.012	0.967	0.394	0.964	0.541	0.106	0.911	0.932	0.685	0.909	0.701
T11	0.010	0.953	0.436	0.975	0.130	0.042	0.813	0.970	0.651	0.876	0.724
T12	0.010	0.962	0.760	0.975	0.374	0.048	0.925	0.965	0.648	0.940	0.540
A1	0.029	0.986	0.304	0.990	0.513	0.414	0.051	0.976	0.856	0.750	0.388
A2	0.009	0.980	0.697	0.907	0.099	0.234	0.028	0.980	0.806	0.769	0.472
A3	0.006	0.984	0.822	0.918	0.428	0.101	0.070	0.970	0.469	0.770	0.445
A4	0.038	0.983	0.342	0.989	0.464	0.647	0.046	0.975	0.870	0.796	0.392
A5	0.021	0.985	0.149	0.910	0.245	0.867	0.017	0.967	0.582	0.761	0.898
A6	0.012	0.974	0.709	0.775	0.042	0.319	0.018	0.984	0.872	0.779	0.478
A7	0.022	0.986	0.938	0.903	0.443	0.923	0.029	0.949	0.691	0.856	0.283
A8	0.019	0.985	0.406	0.931	0.327	0.231	0.038	0.979	0.770	0.779	0.382
A9	0.015	0.979	0.846	0.900	0.089	0.624	0.024	0.989	0.900	0.782	0.489
A10	0.015	0.985	0.726	0.924	0.186	0.272	0.032	0.986	0.856	0.638	0.472
A11	0.010	0.981	0.355	0.863	0.072	0.197	0.029	0.979	0.529	0.505	0.555
A12	0.010	0.984	0.681	0.915	0.238	0.081	0.052	0.975	0.479	0.655	0.382

TABLE-6
SYNTHESISED COMPOUNDS MIC VALVES AGAINST *Mtb* H37Rv

Compd.	MIC (µg/mL) data (99.9% of *Mtb* H37Rv are killed)							
	7.81	15.62	31.25	62.5	125	250	500	1000
A_1	–	+	+	+	+	+	+	+
A_2	–	–	–	–	–	–	+	+
A_3	–	–	–	–	+	+	+	+
A_4	–	–	–	+	+	+	+	+
A_5	–	–	–	–	–	–	–	–
A_6	–	–	–	–	+	+	+	+
A_7	–	+	+	+	+	+	+	+
A_8	–	–	–	–	–	+	+	+
A_9	–	–	–	–	–	–	–	+
A_{10}	–	–	–	–	–	–	–	+
A_{11}	–	–	–	–	–	–	–	–
A_{12}	–	–	–	–	–	–	–	–

– No inhibition of growth; + Inhibition of growth

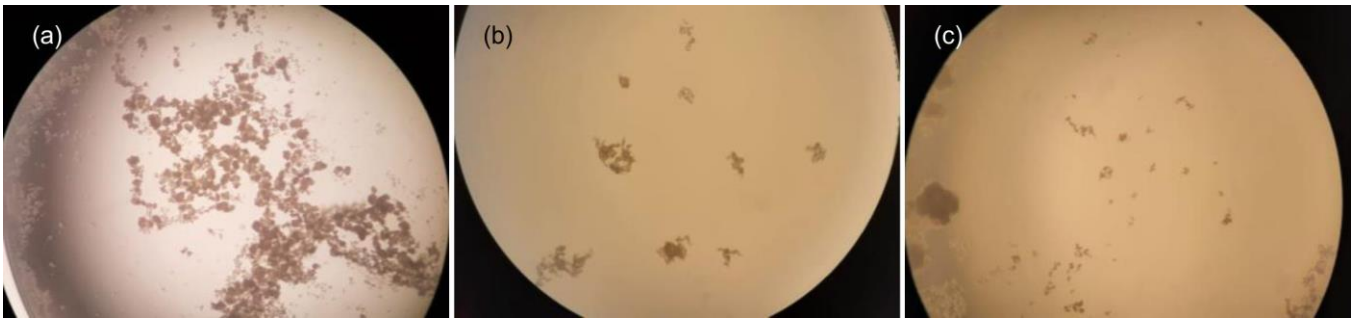

Fig. 5. Nucleoid morphology of *Mtb* H37Rv (fluorescent micrograph): (a) **A_1** at 7.81 µg/mL, (b) **A_{11}** at 7.81 µg/mL and (c) **A_{12}** at 7.81 µg/mL

TABLE-7
% CELL VIABILITY REPORT OF VERO CELL LINES WITH TREATED COMPOUNDS

Conc. (µg/mL)	% of cell viability of Vero cell lines				
	A_1	**A_4**	**A_7**	**A_{11}**	**A_{12}**
100	30	24	16	10	13
50	46	52	36	21	34
25	65	79	59	34	49
12.5	74	100	77	55	69
6.25	82	100	100	88	100
3.125	100	100	100	100	100
IC_{50}	45	45.03	29.97	11.75	20.49
R square	0.955	0.940	0.968	0.981	0.963
P value	0.0007	0.0011	0.0003	0.0001	0.0004
F value	84.22	62.73	122.6	206.8	104.7

by **A_{12}** (20.49 µg/mL) and **A_7** (29.97 µg/mL). Compounds **A_1** (45.00 µg/mL) and **A_4** (45.03 µg/mL) exhibited lower cytotoxicity, corresponding to a comparatively better *in vitro* safety profile.

The selectivity index (SI) of the synthesised compounds was calculated using the formula SI = IC_{50}/MIC, where a higher SI represents greater selectivity toward *M. tuberculosis* over normal mammalian cells. The SI values of compounds **A_1**, **A_4**, **A_7**, **A_{11}** and **A_{12}** were 2.88, 0.72, 1.92, 1.50 and 2.62, respectively. Among the tested compounds, **A_1** and **A_{12}** exhibited relatively higher SI values, exhibited better selectivity and a more favourable safety profile toward normal Vero cells while retaining potent antitubercular activity. **A_4**, **A_7** and **A_{11}** showed lower SI values, corresponding to lower selectivity and comparatively greater cytotoxicity. Based on their antitubercular activity, cytotoxicity and selectivity profiles, **A_1** and **A_{12}** emerged as potential lead compounds for further investigation and development.

Statistical analysis: The statistical analysis indicates that a strong correlation between concentration and cytotoxic response, with R^2 values ranging from 0.940 to 0.981, signifying the reliability of the dose response relationship. Moreover, the F-values (62.73-206.8) and *p*-values (< 0.05) confirmed that the observed effects were statistically significant.

***In vivo* acute toxicity studies:** Acute oral toxicity of compounds **A_1**, **A_4**, **A_7**, **A_{11}** and **A_{12}** was evaluated according to OECD Guideline 423 in male albino mice following the regulations of the Committee for the Control and Supervision of Experiments on Animals (CCSEA), Government of India (IAEC/I/03/RIPER/2022). An initial oral dose of 2000 mg/kg body weight was administered to the animals in each experimental group. All mice receiving this dose died within 4-5 h of administration. Consequently, the dose was reduced to 300 mg/kg body weight. At this dose, all animals survived and remained active throughout the 14-day observation period without any observable signs of toxicity. Based on these findings, the LD_{50} of the tested compounds was estimated to be 300 mg/kg body weight.

At the end of the 14-day observation period, mice from the control and treatment groups were humanely sacrificed, and the heart, kidney and liver were carefully excised for histopathological evaluation. Histological examination of

these organs from the control and treated groups (**A_1**, **A_4**, **A_7**, **A_{11}** and **A_{12}**) was performed to investigate possible tissue toxicity (Fig. 6).

Heart sections from the control group (C H) exhibited normal myocardial architecture with intact and well-organised cardiac muscle fibres. A comparable histological appearance

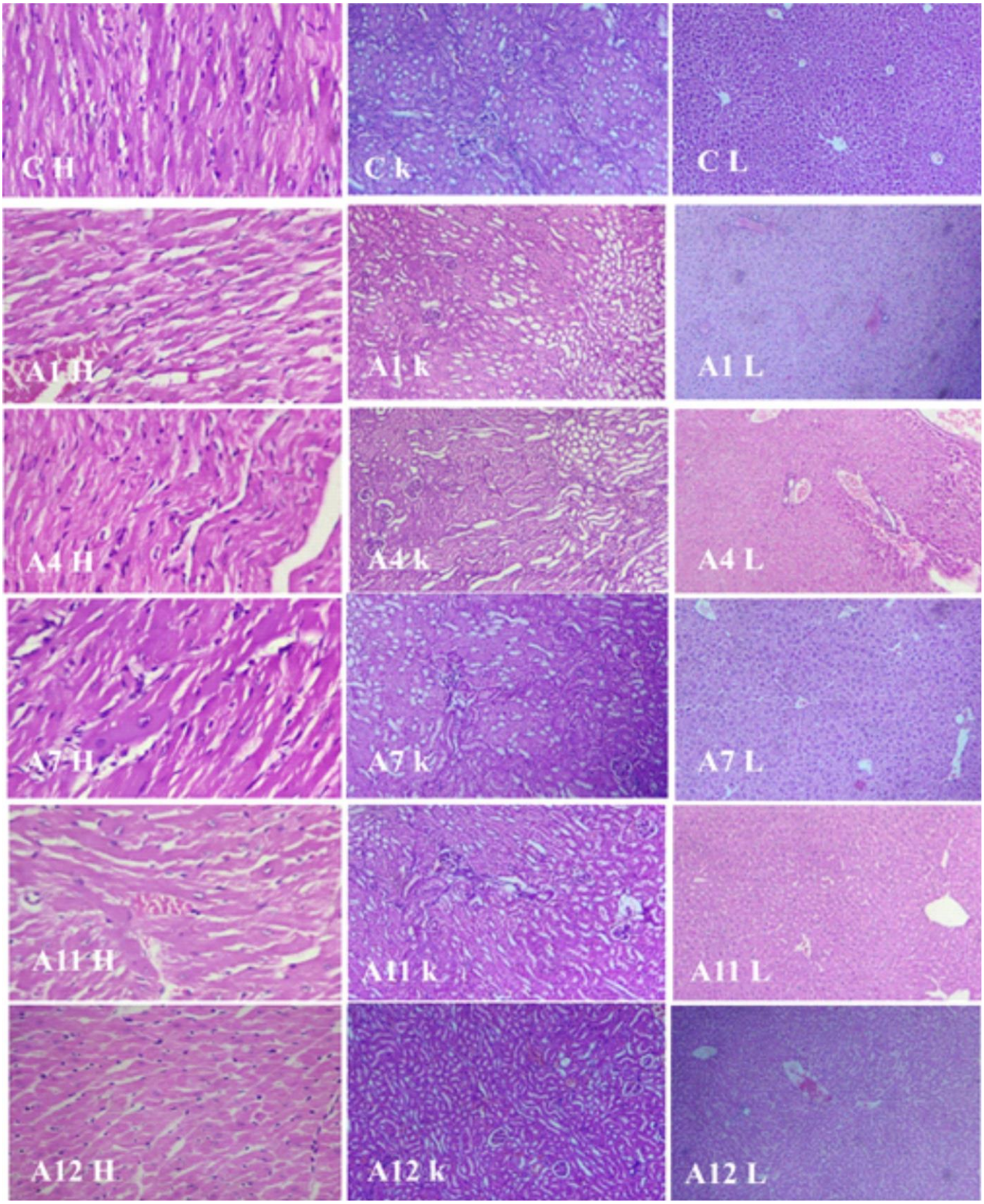

Fig. 6. Isolated heart, kidney and liver histopathological examination of control and treated (**A_1**, **A_4**, **A_7**, **A_{11}** and **A_{12}**) mice

was observed in all treatment groups, with no evidence of cardiomyocyte degeneration, necrosis, inflammatory cell infiltration or other pathological alterations. Kidney sections from the control group (C K) displayed normal glomerular and tubular architecture without histopathological abnormalities. Renal tissues from mice treated with **A1**, **A4**, **A7**, **A11** and **A12** exhibited histological features comparable to those of the control group, with no evidence of glomerular atrophy, tubular degeneration, inflammatory infiltration or structural damage. Liver sections from the control group (C L) showed normal hepatic lobular architecture with well-preserved hepatocytes and intact central veins. Similar hepatic morphology was observed in all treated groups, with no significant evidence of hepatocellular degeneration, necrosis, steatosis or other treatment-related pathological changes. The absence of discernible histopathological alterations in the heart, kidney and liver at 300 mg/kg body weight supports the acceptable acute safety profile of the selected compounds under the experimental conditions employed.

Structure activity relationship (SAR): Anti-tubercular activity of the synthesised triazolyl-azetidinone derivatives (**A11**-**A12**) was strongly influenced by the electronic characteristics, steric effects, hydrogen-bonding capacity and lipophilicity of the aromatic substituents. Electron-donating substituents containing hydroxyl and alkoxy groups enhanced biological activity, with compounds **A11** and **A12** exhibiting the highest potency (MIC ≤ 7.81 μg/mL). Their superior activity may be attributed to favourable hydrogen-bond interactions with the key PPK2 residues ASN131 and GLU136. In contrast, the presence of strongly electron-withdrawing and sterically bulky substituents, such as 2,4-dichloro group in **A5**, was associated with reduced antitubercular activity, despite its comparatively higher lipophilicity, showing the adverse influence of steric hindrance on target binding. Compounds possessing balanced physicochemical properties, including moderate lipophilicity (LogP), appropriate topological polar surface area (TPSA) and suitable hydrogen-bond donor and acceptor capacities, exhibited superior biological activity. These SARs establish that a balanced combination of electronic properties, steric factors, hydrogen-bonding capability and molecular physico-chemical characteristics is essential for effective PPK2 inhibition and enhanced anti-tubercular activity.

Conclusion

Twelve novel 1,2,4-triazolyl-azetidin-2-one compounds (**A1**-**A12**) have been designed, synthesised successfully in two steps and tested as potential anti-tubercular agents targeting the enzyme polyphosphate kinase 2 (PPK2). The computational analyses revealed their relevance to PPK2 inhibition. A homology model was validated for the *M. tuberculosis* PPK2 enzyme and docking analyses revealed strong and favourable interactions between various compounds and key residues within the active site. ADMET analyses revealed that the compounds have good physico-chemical properties, drug likeness and properties suitable for oral bioavailability. The biological screening confirmed the potential of this scaffold against *Mtb* H37Rv, compounds **A11** and **A12** showed the highest activity (MIC ≤ 7.81 μg/mL), while others showed moderate to low effects depending on substituent patterns. Cytotoxicity testing on Vero cells showed dose-dependent effects and selectivity data suggested that **A1** and **A12** balanced potency and safety. *In vivo* toxicity studies in mice identified an LD_{50} of 300 mg/kg and histopathological examination of major organs revealed no significant damage at tolerated doses. Compounds **A11** and **A12** emerged as particularly attractive lead candidates. Although triazole and azetidinone pharmacophores have been investigated individually and in combination as antimycobacterial scaffolds, the present study distinguishes itself by targeting the non-classical enzyme PPK2 through an integrated structure-based drug discovery approach. The favourable docking interactions of **A11** and **A12** with the key PPK2 residues ASN131, GLU136, LYS75 and ARG127, together with their potent *in vitro* antimycobacterial activity, acceptable cytotoxicity profile and favourable *in vivo* safety, provide strong support for the development of PPK2-targeted triazolyl-azetidinones as a new class of lead compounds for antitubercular drug discovery.

ACKNOWLEDGEMENTS

The authors gratefully acknowledge the financial support from AICTE-RPS (F. No: 8.73/RIFD/RPS (policy-1)/2016-17) and the DST-FIST facility at RERDS-CPR, RIPER (Autonomous), Anantapur, India. Thanks are also due to Dr. Azger (NIRT, Chennai) for anti-tubercular activity, Mr. Prakash M.G. (Prakash Diagnostic & Histotech Lab, Bangalore) for histopathology interpretation and SAIF, Panjab University, for NMR and Mass characterisation.

CONFLICT OF INTEREST

The authors declare that there is no conflict of interests regarding the publication of this article.

DECLARATION OF AI-ASSISTED TECHNOLOGIES

During the preparation of this manuscript, the authors used an AI-assisted tool(s) to improve the language and no data, results or scientific conclusions were generated by AI. All analyses, interpretations and conclusions are the authors' own. The authors reviewed and edited the content and take full responsibility for the published work.

REFERENCES

1. S.A. Patil, S.A. Patil, T. Fariyike, K.O. Marichev, H.M. Heras Martinez and A. Bugarin, *Future Med. Chem.*, **13**, 1907 (2021); https://doi.org/10.4155/fmc-2021-0193
2. M.A. Gun, B. Bozdogan and A.Y. Coban, *Future Microbiol.*, **15**, 937 (2020); https://doi.org/10.2217/fmb-2019-0318
3. C.N. Wivagg, R.P. Bhattacharyya and D.T. Hung, *J. Antibiot. (Tokyo)*, **67**, 645 (2014); https://doi.org/10.1038/ja.2014.94
4. I.E. Głowacka, M. Grabkowska-Drużyc, G. Andrei, D. Schols, R. Snoeck, K. Witek, S. Podlewska, J. Handzlik and D.G. Piotrowska, *Int. J. Mol. Sci.*, **22**, 8032 (2021); https://doi.org/10.3390/ijms22158032
5. J.O. Ombito and G.S. Singh, *Mini Rev. Org. Chem.*, **16**, 544 (2019); https://doi.org/10.2174/1570193X15666180914165303

6. S.D. Joshi, U.A. More, D. Parkale, T.M. Aminabhavi, A.K. Gadad, M.N. Nadagouda and R. Jawarkar, *Med. Chem. Res.*, **24**, 3892 (2015); https://doi.org/10.1007/s00044-015-1432-7
7. B. Sravanthi, G. Himavathi, A.R. Robert, P. Karunakar, K.S. Kiran and S. Maddila, *J. Biomol. Struct. Dyn.*, **42**, 5376 (2024); https://doi.org/10.1080/07391102.2023.2226743
8. Z. Karczmarzyk, M. Swatko-Ossor, W. Wysocki, M. Drozd, G. Ginalska, A. Pachuta-Stec and M. Pitucha, *Molecules*, **25**, 6033 (2020); https://doi.org/10.3390/molecules25246033
9. A. Brandi, S. Cicchi and F.M. Cordero, *Chem. Rev.*, **108**, 3988 (2008); https://doi.org/10.1021/cr800325e
10. D.K. Mehta, R. Chaurasiya and R. Das, *Med. Chem.*, **21**, 761 (2025); https://doi.org/10.2174/0115734064355361241230063744
11. R.B. Bakr and N.A. Elkanzi, *J. Heterocycl. Chem.*, **57**, 2977 (2020); https://doi.org/10.1002/jhet.4009
12. K.H. Patel and A.G. Mehta, *J. Chem.*, **3**, 103 (2006); https://doi.org/10.1155/2006/787638
13. P.D. Mehta, N.P. Sengar and A.K. Pathak, *Eur. J. Med. Chem.*, **45**, 5541 (2010); https://doi.org/10.1016/j.ejmech.2010.09.035
14. H. Hasan, M. Akhter, W. Akhter, I. Ali, M. Zaheen, I. Ahsan and D. Mahmood, *Med. Chem. Res.*, **20**, 1357 (2011); https://doi.org/10.1007/s00044-010-9485-0
15. S. Saini, *Drug Res.*, **69**, 445 (2019); https://doi.org/10.1055/a-0809-5098
16. S. Kumar Gupta and A. Mishra, *Antiinflamm. Antiallergy Agents Med. Chem.*, **15**, 31 (2016); https://doi.org/10.2174/1871523015666160210124545
17. M. Dragan, C.D. Stan, A.T. Iacob, O.M. Dragostin, M. Boanca, C.E. Lupuşoru, C.L. Zamfir and L. Profire, *Processes*, **8**, 1401 (2020); https://doi.org/10.3390/pr8111401
18. M.C. Yerigeri, S.K. Murari, K.N. Thimmaiah, S.K.S. Math and B.S. Vishwanath, *Med. Chem.*, **4**, 190 (2008); https://doi.org/10.2174/157340608783789149
19. M. Himaja, A. Karigar, M.V. Ramana, D. Munirajasekhar and S.M. Sikarwar, *Lett. Drug Des. Discov.*, **9**, 611 (2012); https://doi.org/10.2174/157018012800673038
20. K.I. Slavova, L.T. Todorov, N.P. Belskaya, M.A. Palafox and I.P. Kostova, *Recent Pat. Anticancer Drug Discov.*, **15**, 92 (2020); https://doi.org/10.2174/1574892815666200717164457
21. N. Poonia, A. Kumar, V. Kumar, M. Yadav and K. Lal, *Curr. Top. Med. Chem.*, **21**, 2109 (2021); https://doi.org/10.2174/1568026621666210913122828
22. L. Popiołek, *Biomed. Pharmacother.*, **163**, 114853 (2023); https://doi.org/10.1016/j.biopha.2023.114853
23. K.T. Potts, *Chem. Rev.*, **61**, 87 (1961); https://doi.org/10.1021/cr60210a001
24. M. Strzelecka and P. Świątek, *Pharmaceuticals*, **14**, 224 (2021); https://doi.org/10.3390/ph14030224
25. A. Abdelli, S. Azzouni, R. Plais, A. Gaucher, M.L. Efrit and D. Prim, *Tetrahedron Lett.*, **86**, 153518 (2021); https://doi.org/10.1016/j.tetlet.2021.153518
26. S. Maddila, R. Pagadala and S.B. Jonnalagadda, *Lett. Org. Chem.*, **10**, 693 (2013); https://doi.org/10.2174/15701786101031126115448
27. G. Mancuso, A. Midiri, S. De Gaetano, E. Ponzo and C. Biondo, *Microorganisms*, **11**, 2277 (2023); https://doi.org/10.3390/microorganisms11092277
28. A.S. Dean, O. Tosas Auguet, P. Glaziou, M. Zignol, N. Ismail, T. Kasaeva and K. Floyd, *Lancet Infect. Dis.*, **22**, e191 (2022); https://doi.org/10.1016/S1473-3099(21)00808-2
29. S.M. Hassanian, A. Avan and A. Ardeshirylajimi, *J. Thromb. Haemost.*, **15**, 213 (2017); https://doi.org/10.1111/jth.13580
30. T.M. Livermore, C. Azevedo, B. Kolozsvari, M.S. Wilson and A. Saiardi, *Biochem. Soc. Trans.*, **44**, 253 (2016); https://doi.org/10.1042/BST20150215
31. C. Azevedo and A. Saiardi, *Biochem. Soc. Trans.*, **44**, 13 (2016); https://doi.org/10.1042/BST20150210
32. L. Achbergerová and J. Nahálka, *Microb. Cell Fact.*, **10**, 63 (2011); https://doi.org/10.1186/1475-2859-10-63
33. M. Singh, P. Tiwari, G. Arora, S. Agarwal, S. Kidwai and R. Singh, *Sci. Rep.*, **6**, 26900 (2016); https://doi.org/10.1038/srep26900
34. P. Wiji Prasetyaningrum, A. Bahtiar and H. Hayun, *Sci. Pharm.*, **86**, 25 (2018); https://doi.org/10.3390/scipharm86020025
35. M. Alhaji Isa and R. Singh Majumdar, *J. Proteins Proteom.*, **10**, 55 (2019); https://doi.org/10.1007/s42485-019-00006-w
36. L.E. Batten, A.E. Parnell, N.J. Wells, A.L. Murch, P.C. Oyston and P.L. Roach, *Biosci. Rep.*, **36**, e00294 (2016); https://doi.org/10.1042/BSR20150203
37. H.B. Uchôa, G.E. Jorge, N.J. Freitas Da Silveira, J.C. Camera Jr., F. Canduri and W.F. De Azevedo Jr., *Biochem. Biophys. Res. Commun.*, **325**, 1481 (2004); https://doi.org/10.1016/j.bbrc.2004.10.192
38. S. Mordhorst, J. Singh, M.K. Mohr, M. Hinkelmann, H.J. Keppler, J.N. Jessen and J.N. Andexer, *Chembiochem*, **20**, 1019 (2019); https://doi.org/10.1002/cbic.201800704
39. R. Das, D.K. Mehta and M. Dhanawat, *Drug Res.*, **71**, 355 (2021); https://doi.org/10.1055/a-1481-7879
40. R.A. Friesner, J.L. Banks, R.B. Murphy, T.A. Halgren, J.J. Klicic, D.T. Mainz, M.P. Repasky, E.H. Knoll, M. Shelley, J.K. Perry, D.E. Shaw, P. Francis and P.S. Shenkin, *J. Med. Chem.*, **47**, 1739 (2004); https://doi.org/10.1021/jm0306430
41. A. Zindoga, M.Phil. Dissertation, Structure-Based Hit-to-Lead Design, Optimization and Synthesis of Tetrahydro-1,3,5-Triazine-2-Amine Derivatives as Potential Inhibitors of *Mycobacterium tuberculosis* Dihydrofolate Reductase (MtbDHFR), Chinhoyi University Technology, Chinhoyi, Zimbabwe (2023).
42. G. Xiong, Z. Wu, J. Yi, L. Fu, Z. Yang, C. Hsieh, M. Yin, X. Zeng, C. Wu, A. Lu, X. Chen, T. Hou and D. Cao, *Nucleic Acids Res.*, **49(W1)**, W5 (2021); https://doi.org/10.1093/nar/gkab255
43. A.M. Abu-Dief and I.M. Mohamed, *Beni. Suef Univ. J. Basic Appl. Sci.*, **4**, 119 (2015); https://doi.org/10.1016/j.bjbas.2015.05.004
44. P. Senthilraja and K.J. Kathiresan, *J. Appl. Pharm. Sci.*, **5**, 080 (2015); https://doi.org/10.7324/JAPS.2015.50313
45. O. Bedi and P. Krishan, *Naunyn Schmiedebergs Arch. Pharmacol.*, **393**, 565 (2020); https://doi.org/10.1007/s00210-019-01742-y
46. M.J. Garle, J.H. Fentem and J.R. Fry, *Toxicol. In Vitro*, **8**, 1303 (1994); https://doi.org/10.1016/0887-2333(94)90123-6
47. A. Gupta, P. Majumdar, J. Amit, A. Rajesh, S.B. Singh and M. Chakraborty, *Trends Biomater. Artif. Organs*, **20**, 84 (2006).
48. A.L. Nieminen, G.J. Gores, J.M. Bond, R. Imberti, B. Herman and J.J. Lemasters, *Toxicol. Appl. Pharmacol.*, **115**, 147 (1992); https://doi.org/10.1016/0041-008X(92)90317-L
49. A. Kinsner-Ovaskainen, R. Rzepka, R. Rudowski, S. Coecke, T. Cole and P. Prieto, *Toxicol. In Vitro*, **23**, 476 (2009); https://doi.org/10.1016/j.tiv.2008.12.019
50. U. Ukelis, P.J. Kramer, K. Olejniczak and S.O. Mueller, *Regul. Toxicol. Pharmacol.*, **51**, 108 (2008); https://doi.org/10.1016/j.yrtph.2008.02.002
51. E.O. Erhirhie, C.P. Ihekwereme and E.E. Ilodigwe, *Interdiscip. Toxicol.*, **11**, 5 (2018); https://doi.org/10.2478/intox-2018-0001
52. J.R. Fry, M.J. Garle and A.H. Hammond, *Altern. Lab. Anim.*, **16**, 175 (1988); https://doi.org/10.1177/026119298801600208
53. B.M. Pour, L.Y. Latha and S. Sasidharan, *Molecules*, **16**, 3663 (2011); https://doi.org/10.3390/molecules16053663